Heliyon 10 (2024) e40967

Contents lists available at ScienceDirect

Heliyon

journal homepage: www.cell.com/heliyon

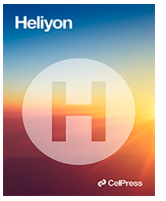

Research article

Adhesion properties of polyimide coated stacks: An in-depth analysis of the cross-sectional nanoindentation method

Moritz Hartleb [a,b,*], Peter Imrich [b], Johannes Zechner [c], Thomas Walter [a], Manuel Petersmann [b], Golta Khatibi [a]

[a] Institute of Chemical Technologies and Analytics CTA, TU Wien, Getreidemarkt 9/164, 1060, Vienna, Austria
[b] KAI-Kompetenzzentrum Automobil- und Industrieelektronik GmbH Technologiepark Villach, Europastraße 8, 9524, Villach, Austria
[c] Infineon Technologies Austria AG, Siemensstraße 2, 9500, Villach, Austria

ARTICLE INFO

Keywords:
Thin films
Delamination
Nanoindentation
Finite element method
Polyimide

ABSTRACT

Adhesion at the interface between dissimilar materials in the semiconductor industry is an important topic, but reliable quantitative methods for strongly adhesive or highly plastic layers are hardly available. This study aims to investigate the suitability of the cross-sectional nanoindentation (CSN) method for determination of the critical energy release rate of thin film stacks in the presence of a polyimide layer as a representative structure for such a case. For this purpose, the adhesion of a deliberately weakened Si/SiO_x interface in a Si/SiO_x/Al/Si_xN_y/polyimide stack is examined by systematic variation of the experimental parameters. This allows for a limitation of the plastic energy dissipated in the polyimide layer during delamination, while still investigating its influences on the overall delamination behavior. The results and evaluability of individual experiments were strongly affected by the geometry of the indenter tip and the distance of indentation to the interface, while other internal control parameters of the nanoindenter were more relevant for ease of the experimental procedure. An optimized choice of the mentioned parameters, 8 µm distance from the deposited layers for the cube-corner tip geometry, and 10 µm for the Berkovich geometry, led to 30 % of evaluable results, considered as high for quantitative adhesion testing of thin films. A multi-stage finite element analysis was developed to consider the effect of plasticity in the polyimide layer. Using this, the critical energy release rates (G_c) of the Si/SiO_x interface was determined to be 9.61 J/m^2 and 10.85 J/m^2 for the cube-corner and Berkovich tip geometries, respectively. This work presents a novel promising way to extend the application fields of the CSN method for the determination of the energy release rate of systems containing layers with a high plasticity.

1. Introduction

In the realm of component-reliability of thin film systems, delamination along dissimilar layers induced by e.g., differences in the coefficient of thermal expansion is a critical issue which has been subject of intensive research [1]. To study this phenomenon a variety of testing techniques have been developed, which aim to induce delamination within the interfaces of the multilayered systems. Depending on the research question, different qualitative or quantitative methods are available. While qualitative tests serve to

* Corresponding author. Institute of Chemical Technologies and Analytics CTA, TU Wien, Getreidemarkt 9/164, 1060, Vienna, Austria.
E-mail address: moritz.hartleb@tuwien.ac.at (M. Hartleb).

https://doi.org/10.1016/j.heliyon.2024.e40967
Received 6 August 2024; Received in revised form 22 October 2024; Accepted 4 December 2024
Available online 7 December 2024

conduct comparative analysis among two or more systems of interest [2], the quantitative methods provide values for the adhesion strength e.g., in the form of a force per area needed to achieve delamination or the interfacial fracture toughness, a measure of the energy required for a crack to advance based on analytical solutions [3]. Finite element analysis (FEA) is used for a more accurate assessment of the adhesion properties of complex multilayered structures.

A number of standard test procedures are available for certain multilayered systems such as coatings (e.g., Refs. [4–6]). Yet no universal technique is available for adhesion testing of thin film stacks, especially for strongly adhering layers where only few methods produce reliable results. Four-point bending [7] or the double cantilever beam methods using sandwich type specimens are often used for measuring the adhesion strength of thin films on rigid substrates. However, the fabrication of sandwich specimens, which requires the bonding of two opposing specimen strips by using a glue (e.g., Ref. [8]), is not only time-consuming, but undesirable failure modes such as cracking of the brittle substrate or failure at the bonded interface can also occur [2] which leads to a low output of evaluable experiments. Scratch testing to induce delamination is an alternative method to quantify the adhesion but is restricted to certain combinations of films and substrates [8]. Furthermore, the peel test, another widely used method that is relatively straightforward to perform [9], fails if the cohesive strength of the peeled layer is surpassed. In addition, application of these methods for investigations of semiconductor samples on a macroscopic scale require specially processed specimens, as the area needed for testing far exceeds the unstructured area available in the real products. The cross-sectional nanoindentation (CSN) method, first described by Sánchez [10], does not depend on external adhesives as needed for sandwich samples and works on a microscopic level, enabling the investigations of structured components. However, since plasticity in deforming layers is not taken into account in the originally proposed analytical solutions, the energy consumption due to the significant plastic zone around the crack tip [11] is not considered. This leads to inaccurate values for the critical energy release rate unless FEA simulations are used to account for additional mechanisms of energy dissipation. Specifically, FEA allows to divide the energy invested into the system into two parts: the plastically dissipated energy and the energy invested to advance the crack during the delamination process.

Due to its use as a passivation layer with high chemical and mechanical stability [12], polyimide is a key material in the semiconductor industry. Adhesion properties of polyimides to various metallic layers (Cr, WTi, Ti) have been studied in a number of studies [12–14]. Using the tensile induced delamination method, where the polyimide layer serves as the substrate, critical energy release rate values ranging from 2 J/m^2 to 5 J/m^2 have been reported. On the other hand, critical energy release rates of 100 J/m^2 or more, were found for the adhesion of dielectrics such as SiO_2 [15] or Si_xN_y [16] to polyimide as determined by laser spallation and double cantilever bending techniques.

The aim of this study is the assessment of CSN for the quantitative evaluation of semiconductor thin film stacks in the presence of a polyimide layer. In a recent study by the authors [17], adhesion properties of a $Si/SiO_x/Al/Si_xN_y$/polyimide system were investigated by the CSN method. The purpose of the experiment was to induce delamination along the Si/SiO_x interface to observe the influence of the presence of a 6 μm thick polyimide coating without a direct delamination of this layer. The study showed promising first results by applying FEA to support the CSN measurements. This calculation made it possible to correct the non-elastic effects to avoid the erroneous increase of the calculated energy values. However, it was observed that the induced cracks deviated from the desired Si/SiO_x interface after propagating for a certain distance. The short length of the interface crack led to an inaccurate value of the energy required for crack propagation during the testing. Due to the good adhesion of the thermally grown silicon oxide layer to the silicon substrate commonly encountered in semiconductor components, there exist no reference values for the critical energy release rate of the interface in pristine conditions. However, a number of G_c values for the adhesion of a variety of thin layers, commonly deposited on the silicon oxide layer have been reported. For the adhesion of a SiO_x film to a Si_xN_y film for example, critical energy release rate values were found to be in the range of 1.5 J/m^2 [10] as determined by cross-sectional nanoindentation. A similar value of 1.9 J/m^2 was obtained for a TiN to SiO_x interface [18] using the superlayer method. For the adhesion of a tungsten layer to SiO_x a significantly higher G_c of 9.5 J/m^2 [19] was obtained by indentation adhesion tests, while expectedly low values of 0.1–2 $J/m^2$for the adhesion of copper to the silicon oxide layer were reported [19].

Based on an extensive experimental matrix and FE modeling, this follow-up study aims to improve the understanding of the key points of the CSN method and extend its application to systems consisting of layers which do not show a purely elastic behavior. To achieve this, the potential influence of varying the experimental parameters, specifically.

(i) Distance to the interface
(ii) Loading rate
(iii) Tip geometry

was investigated to determine the optimal conditions for a high experimental success rate by provoking long and stable cracks, while minimizing damage in the deposited layers that often accompany the delamination event and prevent an accurate quantification. In a second step, the influence of the stress singularity at the crack tip [20] on the results obtained via a previously established FEA procedure at different mesh-sizes has been investigated. This allowed to obtain mesh-size independent results for the corrected energy release rate without the necessity of dynamic remeshing [21], which is not applicable for the used simulation technique. Finally, the effect of secondary parameters like angle of incidence of the crack on the interface, mode mixity at the crack tip and plastic zone size around the point of indentation are investigated and discussed. This provides additional insights into the procedure of the CSN experiment, relevant for all systems which contain layers that show significant plasticity.

2. Materials and methods

2.1. Materials

The material stack used for this study is composed of a 750 μm thick Si-substrate that is heavily As doped (As concentration of $4 \cdot 10^{19}$ cm^{-3}), followed by a thermally grown silicon oxide (SiO_x) layer with a thickness of 100 nm, a 300 nm thick Al metallization deposited via magnetron sputtering, a 40 nm thick silicon nitride (Si_xN_y) layer deposited by chemical vapor deposition and a 6 μm thick polyimide layer that was applied via spin coating and subsequently cured. Fig. 1 shows the resulting thin film layered system as seen in a scanning electron microscope (SEM). Due to the non-standard combination of highly As doped substrate combined with the thick oxide layer, the crack grows preferably along the Si/SiO_x interface.

2.2. Methods

2.2.1. Sample preparation

Samples were received in the form of thin strips of size 14×8 mm^2 already cut by a conventional wafer saw along the (010)-crystal plane and then further broken into smaller pieces to fit the fixture used for the CSN experiment. In order to prepare sufficiently smooth sample edges to facilitate long and stable crack growth, additional polishing was conducted by using a Hitachi ArBlade 5000 ion-slicer. The ion-slicer operated with an acceleration voltage of 8 kV, discharge voltage of 2 kV and an argon gas flow rate of 0.13 cm^3/s. Due to the considerable heat introduced into the sample during this process, the relevant layers were shielded by exposing the Si substrate to the ion beam. The time for ion polishing a cross-section with these settings was approximately 4 h. A single cross-section was suitable for approximately 10 indentation experiments.

The experiments were conducted by using a KLA G200 XP Nano Indenter®. Special sample holders were machined to keep the polished wafer pieces in an upright position without hindering the delamination induced during the experiments. This was facilitated by pressing a small strip of aluminum oxide, with a height of 6 mm, against the sample via two eccentric screws as seen in Fig. 2. The sample holder was then placed in the nanoindenter to proceed with the CSN experiments. The interfaces need to be aligned parallel to the lower edge of the nanoindeter tip to ensure symmetrical crack propagation. This setup was manually executed with the aid of a light microscope integrated into the nanoindenter using a ×50 objective lens. Consistency was maintained throughout all experiments by ensuring that the sample fixture was neither moved nor modified during the investigations, with samples being inserted only via the mechanism described above.

2.2.2. Cross-sectional nanoindentation

CSN works by pressing a diamond tip with a triangular base into the substrate of a material stack, near the layers of interest for which the interfacial fracture toughness is to be determined normal to their thickness dimension. Care must be taken to align one edge of the tip precisely parallel to the examined layers of the stack. As the load increases, the diamond tip is pushed further into the material until cracks originate from the corners closest to the interface, at the so-called pop-in load [22], and subsequently travel towards the deposited layers. This causes a piece, or wedge, of the substrate to fracture out of the bulk material, which is pressed against the deposited thin film layers under subsequent loading of the nanoindenter tip. If kinking of the cracks into the interfaces between the thin film layers is energetically favorable, as described by He and Hutchinson [20], further displacement of the wedge towards the deposited layers via the indenter tip causes delamination in the shape of a semi-circular buckle. Fig. 3(a) provides a schematic illustration of the CSN procedure giving an overview of the created delamination buckle as well as movement direction of the indenter tip and silicon wedge relative to the sample. The energy release rate can be calculated using the method described by Sanchez [11] with the aid of

$$G_{analytic} = \frac{D \cdot (1-\nu^2) \cdot u_0^2 \cdot (1-\lambda)^4 \cdot (2F + \lambda \cdot F)}{(a-b)^4} \tag{1}$$

Where D denotes the flexural rigidity of the plate, ν the Poisson's ratio, a the crack length, b the width of the fractured silicon wedge,

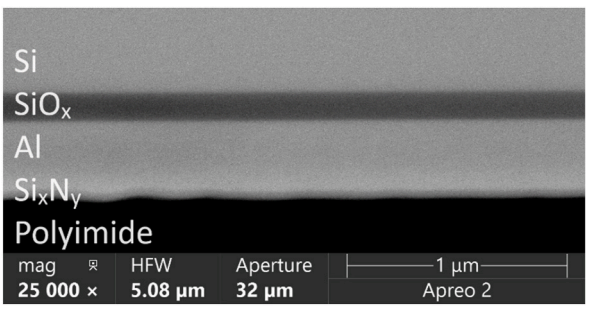

Fig. 1. SEM image of investigated layer stack for Si/SiO_x adhesion.

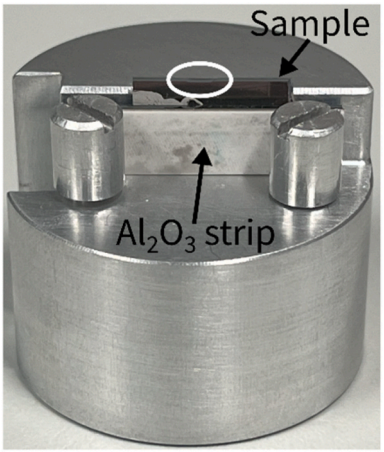

Fig. 2. Sample holder used to keep samples fixed in upright position. The white circle shows the polished area used for indentation experiments.

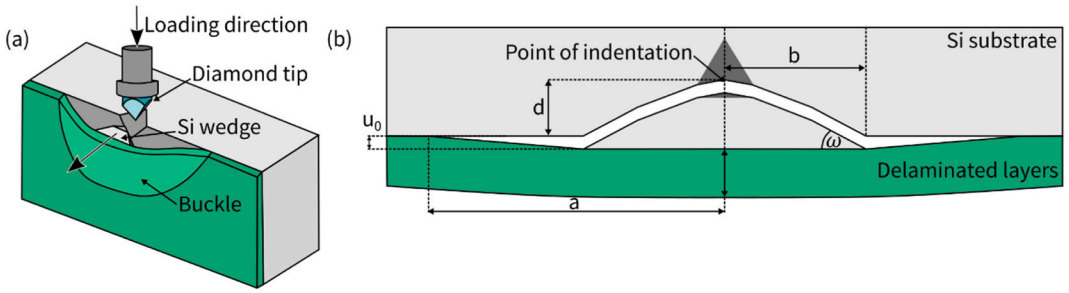

Fig. 3. Schematic drawing depicting the CSN process; (a) growth of a semicircular buckle by pressing the pyramidal indenter into the substrate (b) resulting geometry as seen from the top depicting all relevant parameters gathered by SEM adapted from Ref. [17].

$\lambda = a/b$ and u_0 the maximum wedge displacement during the experiment. F is given by eq (2) and $F' = dF/d\lambda$ is the derivative with respect to λ.

$$F(\lambda) = \frac{2 \cdot ln\,\lambda + \frac{1+\lambda}{1-\lambda} \cdot ln^2\lambda}{((1+\lambda) \cdot ln\,\lambda + 2(1-\lambda))^2} \tag{2}$$

The parameters a, b and u_0 are schematically shown in Fig. 3 (b). They can be readily obtained using SEM imaging, which in this study was performed using a Thermo Scientific Apreo 2 S scanning electron microscope. While eq. (1) does not explicitly contain the distance to the interface d (compare Fig. 3), the dependency is implicitly given through influences on both, the width of the silicon wedge and the final crack length. The major impact of the distance on the results are described later. As the nanoindenter used in this study is load-controlled, any elastic energy stored in the device's spring system is converted into kinetic energy at the pop-in load. It is therefore not possible to stop the tip immediately and thus set an exact halt point for the crack progression.

Since the used G200 Nano Indenter® allows the programming of customized routines, adjustments were made to the CSN test procedure to allow for easy access to relevant control parameters such as indenter tip speed and loading rate. Furthermore, a user-defined criterion was introduced to terminate the CSN experiment after delamination, which was triggered when the indenter tip reached a critical velocity. This critical velocity is referred to below as the velocity cut-off.

In addition to varying the distance d shown in Fig. 3, which is known to alter the geometry of created indents [10], two additional parameters, the loading rate and velocity cut-off were varied to evaluate their effects on the stability of crack propagation and thus on the success rate of the CSN experiment. Finally, multiple indents were performed using a cube-corner tip (halfangle of $\Theta_{CC} = 35.3°$) instead of the more commonly used Berkovich tip (halfangle of $\Theta_{Berk} = 65.3°$), to investigate the possible effects of the different tip

Table 1
Testing parameters with investigated settings for distance of indentation point to interface, loading rate and velocity cut-off.

Nominal Distance (μm)	Loading rate (mN/s)	Velocity cut-off (nm/s)
8–12	200–5000	50–800

geometries. The details of the investigated settings are given in Table 1.

2.2.3. Finite element analysis

In previous studies [17,23,24] it was shown that eq. (1) is based on two assumptions which apply only to purely elastic stacks [17]. Firstly, the equation is based on linear elastic fracture mechanics [23], implying that there is no plastic dissipation of the energy during the CSN experiment. In our stack both, the Al layer as well as the polyimide layer, exhibit significant plasticity, which would cause overestimation of the energy release rate [25]. Secondly, it is assumed that the observed wedge displacement u_0, measured after testing in the SEM is the same as the maximum during testing. However, it was found that the wedge displacement actually decreases after the test due to the relaxation of the separated segment. For this stack, the average u_0 decreases by approximately 80 % [17].

For investigations of bimaterial crack growth, the virtual crack-closure technique (VCCT) is often used as it allows for mode separation of the energy release rate [26–28]. However, the method is based on linear elasticity [29] which cannot be guaranteed for the current system, hence a different approach needed to be chosen. Elizalde et al. [23] were the first to introduce a method suitable for CSN, which is able to separate the influence of plasticity using FEA and energy conservation principles. The method is based on the energy derivative technique [30], which considers the complete loading history of the material even under extensive plastic deformation of materials in the stack. The current method consists of two separate simulations: a load-controlled simulation followed by a displacement-controlled simulation. Simulations were performed in Ansys Mechanical APDL 2022 R2, using axisymmetric, four-sided quad elements with quadratic shape functions for the Si-wedge and linear shape functions for the deposited layers. Table 2 shows the relevant material properties for the simulation, considering plastic deformation for the Al and polyimide layer, while the other layers behave purely elastically. To describe the plasticity for the Al layer a bilinear hardening model has been employed, as is commonly found in literature, e.g. Refs. [31–33], while for the polyimide a multilinear model has been chosen to represent hardening. Examples of such hardening are given in, e.g., Refs. [34–36].

For each simulation the geometry of the observed fracture is first drawn in the software according to the values for wedge width, crack length, and the distance of the indentation to the interface obtained by SEM investigations and shown in Fig. 4. This way, the individual shape of the silicon wedge, based on the wedge width and the distance to the interface is represented for each indentation experiment. The substrate (except for the fractured wedge) is considered a rigid body and is therefore omitted from the model. During both types of simulations all nodes along the crack path are initially fully constrained in all their degrees of freedom, representing the state of the sample before cracks reach the deposited layers. Nodal degrees of freedom constraints are then deleted in succession to simulate the crack growth in the interface. In the load-controlled simulation the normal component of the pop-in load [37], as detected by the load plateau of the nanoindenter, is used as an input for the load in the simulation and applied in the direction as indicated in Fig. 4 until all nodal constraints have been removed, corresponding to the final crack length that is experimentally observed. In the last simulation step the load is removed to obtain information on the unloading behavior. Performing such a simulation allows to obtain the displacement of the silicon wedge during each step of the simulation, which cannot be taken as linearly increasing due to hardening of the deposited layers. The displacement values obtained in the load-controlled simulation can be used as an input for the displacement-controlled simulation allowing a more faithful recreation of the performed indentation experiment.

The load-controlled simulation result is validated by comparing the final simulated value of displacement obtained after load-removal with the experimentally observed wedge displacement. If the discrepancy to the experiment is not within a threshold (±5 % in this study), the load-controlled simulation is performed again with adjusted force values until a match with the measured u_0 is found. This is done as the wedge-displacement is the more easily accessible parameter, while the calculation of the normal force relies on various assumptions and is more prone to errors. If no match can be found within a certain number of iterations (here 10 load-controlled simulations), the simulation is aborted, the evaluation dismissed and the experiment that was recreated in the software not included in the final result.

If the load-controlled simulation is successfully performed, a follow-up displacement-controlled simulation is performed to determine the critical energy release rate. In this simulation the wedge-displacement and crack-growth are applied in separate sub-steps. This is necessary to satisfy the requirements for applying the energy derivative technique approach. In general, the energy release rate G due to energy conservation is given as

$$G = -\frac{\Delta(E-W)}{\Delta A} = \frac{\Delta W}{\Delta A} - \frac{\Delta E}{\Delta A} \tag{3}$$

with ΔW the external work done, in this case by the nanoindenter tip, ΔE the change in total strain energy, by summing over all elements in the mesh, and ΔA the increase in crack length.

By setting up the simulation in two steps the crack growth can be fully confined to constant displacement conditions. In the first step

Table 2
Material properties used for FEA.

Materials	Young's modulus (GPa)	Poisson's ratio	Source	Hardening behavior
Si < 100>	186	0.27	[17]	None
SiO_x	60	0.20		None
Al	80	0.20		Bilinear
Si_xN_y	314	0.28		None
Polyimide	2.05	0.35		Multilinear

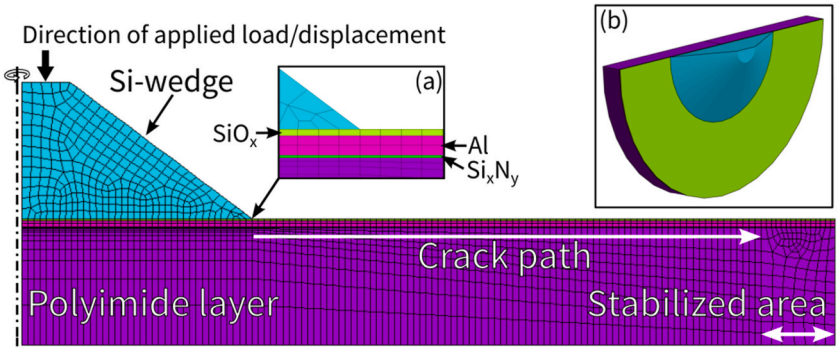

Fig. 4. Geometry used for FEA simulations at one mesh size showing the crack path and the stabilizing material beyond the final crack length. The normal component of the load and displacement are applied to the top line of the Si wedge along the direction of the bold arrow. Inset (a) shows a zoomed in version of the thin films in the material stack near the Si wedge, while inset (b) shows the complete geometry created by rotating the mesh around the indicated axis on the left.

external work is done by increasing the displacement increment of the wedge while keeping the crack length constant. This way the strain energy E in the system is increased. In the second step, the displacement is kept constant ($\Delta W = 0$), while the crack is allowed to grow in which case eq. (3) can be rewritten as

$$G_{simulation} = -\frac{\Delta E}{\Delta A} = -\frac{\Delta E_{el} + \Delta E_{pl}}{\Delta A} \tag{4}$$

where ΔE_{el} and ΔE_{pl} are the changes in elastic and plastic energy during the current step and ΔA is the semicircular area that was delaminated in the corresponding step.

Each time the crack is extended, a value for the energy release rate is obtained by using eq. (4)where the critical energy release rate is then obtained from the last step when the crack reaches the length that was experimentally observed after the CSN experiment. At this step, the energy available for delaminating the interface is equal to the energy needed for crack propagation.

In FEA, due to element discretization and the stress singularity at the sharp crack tip, the choice of the element-size has a significant impact on the obtained energy release rate [21]. Choosing smaller elements at the crack tip does not solve the problem readily, as this can lead to divergences in the simulation due to the stress localization.

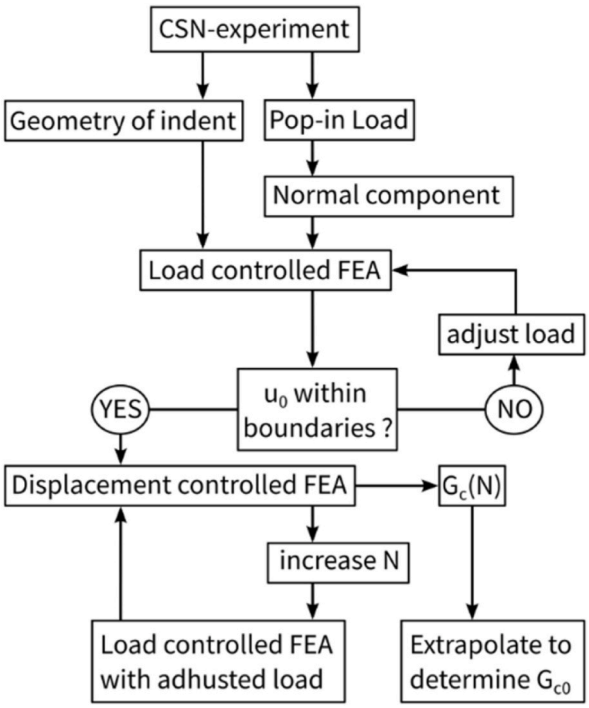

Fig. 5. Algorithm used to obtain energy release rate values from CSN experiments using FEA. N is the number of elements along the crack path.

Two common strategies exist to address this issue: One can resolve the crack tip as rounded, which is not practical here, as a higher resolution of the crack tip in the very thin layers near the cracks would cause an unreasonably fine mesh, making the simulations computationally too expensive. Alternatively, gradient formulations can be utilized, which however introduce an unknown length scale into the problem, which is not known for the current case. To this end an adapted method was devised for this study to address mesh-size dependency.

Multiple simulations, both load-controlled and displacement-controlled, with an increasing number of elements along the crack path were conducted without changing the experimental input. The resulting critical energy release rates from these 'mesh refinement loops' were obtained as described above and ultimately plotted against the number of elements N along the crack path. The obtained data was then fitted using following fit function

$$G_c(N) = A \cdot \exp(-N \cdot \tau) + G_{c0} \tag{5}$$

Where $G_c(N)$ is the result for the critical energy release rate obtained from simulations at a certain number of elements, N is the number of elements along the crack path, A and τ are fit parameters, path and G_{c0} the desired mesh independent critical energy release rate. An example showing the quality of the fit is given in the results. For every such N, a load-controlled simulation was performed beforehand to obtain the displacement behavior, while only for the coarsest mesh, the load-adjustment loops were performed to obtain the suitable input load. The complete algorithm used to perform the FEA simulations is shown in Fig. 5.

Considering this approach, a successful experiment is defined in this paper as one in which the CSN experiment not only led to the expected delamination behavior, but also in which FE simulations of the generated geometry could be performed at successively finer meshes, which are ultimately evaluated in eq. (5).

A further issue when comparing different adhesion test methods is the consideration of mode mixity under which the delamination takes place, as this can strongly influence the obtained critical energy release rate values [20]. The mode mixity, defined as $\psi = tan^{-1}(\tau_{xy}/\sigma_{yy})$ provides the ratio of the shear stress τ_{xy} to the tensile stress σ_{yy} at the crack tip during the delamination process [38], where a pure mode I crack is described by $\psi = 0°$ and a pure mode II crack by $\psi = 90°$ [39]. In this study the possible difference between the mode mixity angles of CSN tests performed using the Berkovich and cube-corner tip was investigated. For this purpose, the shear stress τ_{xy} and the tensile stress σ_{yy}, at the crack tip are recorded for each step of the simulation and evaluated to obtain the mode mixity behavior at the crack tip over the course of the simulation.

3. Results

3.1. Performed experiments and provoked delaminations

A large number of CSN experiments were conducted to provoke cracks along the Si/SiO_x interface by using the cube-corner tip (128 cracks) and the Berkovich tip (116 cracks). To determine the optimal parameters for achieving a high success rate of the experiments, multiple combinations of loading rate (between 200 and 5000 μN/s) and velocity cut-off (between 50 and 800 nm/s) were implemented at three different distances to the interface (8, 10 and 12 μm) for both tip geometries. The extensive experimental matrix can be found in the supplementary material to this paper. In all cases the geometric data of the delamination experiment was extracted via SEM imaging and the semicircular shape of the delamination was confirmed via light microscopy. Fig. 6, shows examples of proper delamination provoked by the two tip geometries, where cracks travel from the point of indentation through the silicon layer into the deposited layers causing delamination. Fig. 6 (a) and 6 (b) shows this for a cube-corner and a Berkovich tip, respectively. The light microscopy images in Fig. 6 show the geometry of the provoked buckles in the polyimide layer and confirm their semi-circular nature as well as damage introduced in the layers. Fig. 7 compares the ideal behavior observed during an experiment (shown in Fig. 7(a)–(c)) to possible errors that can negatively influence the accurate evaluation of the created indents (shown in Fig. 7(d)–(g)). The latter include local plasticity in the polyimide layer (Fig. 7(d)), fractured silicon pieces preventing crack closure (Fig. 7(e)), cracking around

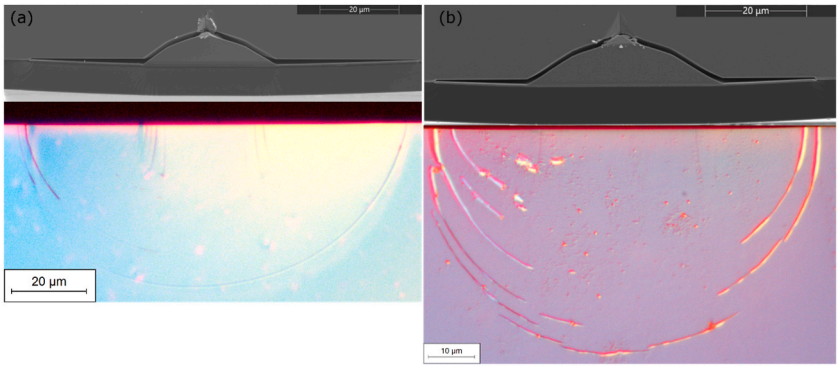

Fig. 6. Delamination induced by CSN captured using SEM (upper row) and respective buckle as seen using light microscopy (lower row); (a) cracks created by cube-corner indenter (b) cracks created by Berkovich indenter.

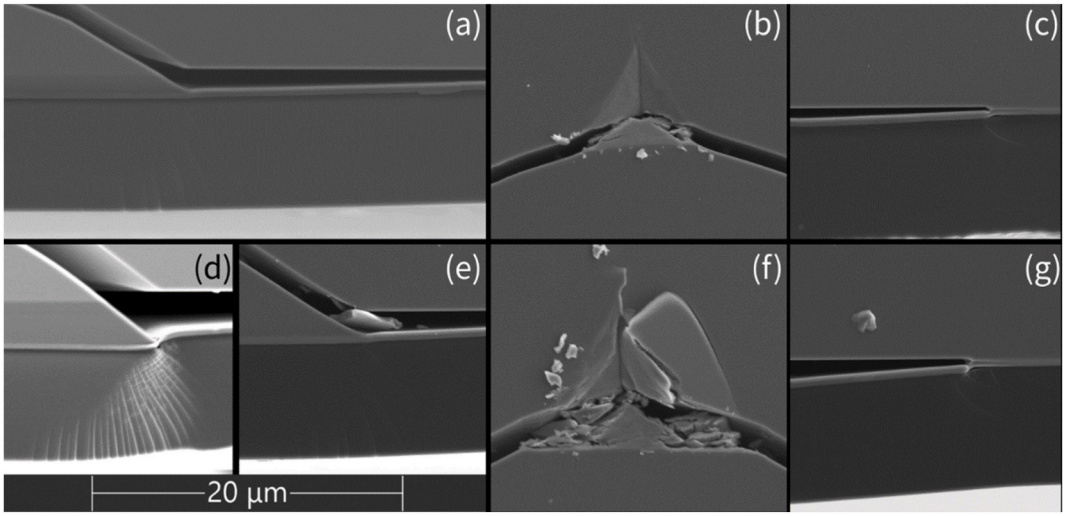

Fig. 7. Examples describing possible effects that can disrupt successful evaluation of experiments; (a)–(c) ideal conditions for successful evaluation of CSN experiments (d) local plasticity seen around the wedge in a cube-corner indent at distance 10 µm from the interface (e) debris wedged inside the crack prevents relaxation in Berkovich indent (f) increased load causes micro cracking around point of indentation in Berkovich indent (g) residual crack opening at the final crack length due to kinking into the Al layer.

the point of indentation (Fig. 7(f)) and cracks kinking into the adjacent layer (Fig. 7(g)).

To better understand the behavior of the indenter tip during the experiment, the velocity was recorded and overlaid with the corresponding load displacement plot, as shown in the representative curve in Fig. 8. In this case, the maximum value for the indenter velocity at which the nanoindenter stops the experiment, the velocity cut-off, was set to 200 nm/s. Due to the load-controlled nature of the G200 Nano Indenter® this value is surpassed significantly as the crack initiates (indicated by the dashed vertical line in Fig. 8) and the energy stored in the springs is transformed into kinetic energy, reaching a value of 9255 nm/s. As this process happens extremely fast, little to no data is acquired during this phase of the experiment. Correspondingly there is lack of data points in this regime in both the load as well as the velocity plot. Fig. 8 nicely shows that the acceleration of the tip and the pop-in event occur simultaneously.

An in-depth analysis of the influence of the three parameters: distance to the interface, maximum load and maximum indenter velocity on each other is shown in Fig. 9, which plots the maximum velocity of the indenter tip against the maximum load, at which cracks were initiated. Different colors of the datapoints indicate different distances of the indentation point to the interface, while the crosses indicate which experiments could be successfully evaluated using the mesh refinement algorithm. Additionally, the increase in the maximum load and velocity with increasing distance for the individual tip geometries is described by the linear fits, showing a steeper incline for the cube-corner geometry than for the Berkovich geometry by a factor of 18.

While also investigated, no correlation between loading rate and final indenter velocity could be found.

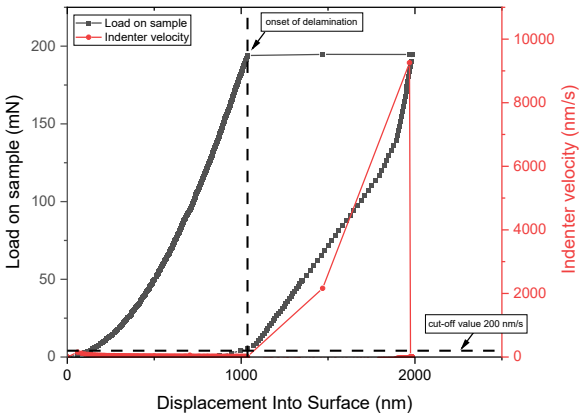

Fig. 8. Load and indenter velocity showing the cut-off criterion set to 200 nm/s. The delamination event can be detected by the pop-in in the load-displacement plot and by the acceleration of the indenter tip in the velocity-displacement plot.

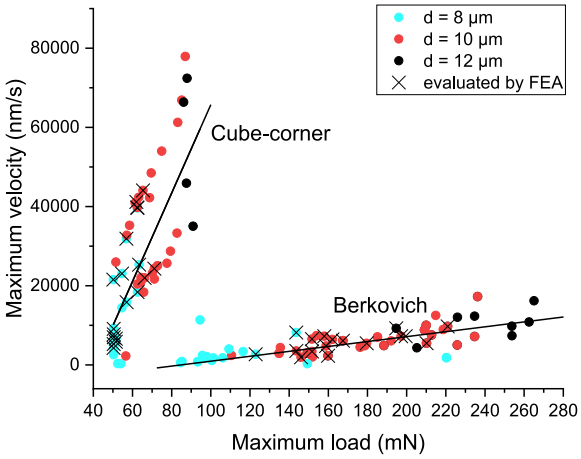

Fig. 9. Dependency of the maximum indenter velocity on maximum load showing distinct differences in the behavior depending on the tip geometry and set distances to the interfaces.

3.2. *Observations for cube-corner tip geometry*

Approximately 18 % of the 128 cracks generated with the cube-corner indenter could be evaluated using the mesh refinement method. The majority of the successfully evaluated cracks were generated with a distance to the interface of 8 µm, while only a few cracks could be evaluated for a distance of 10 µm and none for a distance of 12 µm. Detailed results are presented in the supplementary material. The force needed for crack initiation increases linearly with increasing the distance of the indentation point to the interface. Accordingly, the maximum velocity reached by the indenter head also tends towards higher values. Both effects are shown in Fig. 9. Regardless of the chosen settings, cracks kink into the interface at an angle of $\omega = 35.67 \pm 2.3°$ as measured from obtained SEM images. The experimentally observed crack growth can also be displayed using FEA as is shown in Fig. 10 displaying the crack advancing over time by pushing the Si wedge into the layers in the form of von Mises stress distributions. Alternatively, the von Mises strain is shown in Fig. 11.

At the point where the crack transitions from cohesive to adhesive propagation, local plasticity in the polyimide layer occurs (see Fig. 7(d)), which is more pronounced at greater distances from the interface. In addition, plastic deformation is observed at the crack tip when propagation into the Al layer takes place. Both cases lead to an error by increasing the value of u_0. Quantification of the effect due to kinking into the Al layer, is based on the measurement of the crack tip opening compared to a sharp crack closure, denoted by $\Delta u_{0,ct}$ (see Fig. 7(g)). Similarly, values were corrected for the initial local plasticity around the Si wedge, denoted by $\Delta u_{0,wp}$ (see Fig. 7 (d)), by comparing the indents to the behavior in pristine indentation experiments. The average increase in the wedge displacement due to these two errors is given in Table 3 for the three different chosen distances. For the FEA procedure these errors were considered and corrected for each individual indent if present.

Initial FEA investigations on four indentation experiments using the cube-corner indenter geometry at a distance of 10 µm were performed at 8 different meshes ranging from $N = 82$ to $N = 418$ elements along the crack propagation path, which serve as an example of the good agreement to the exponential fit proposed in eq. (5) and to obtain mesh size independent values. Results of critical energy

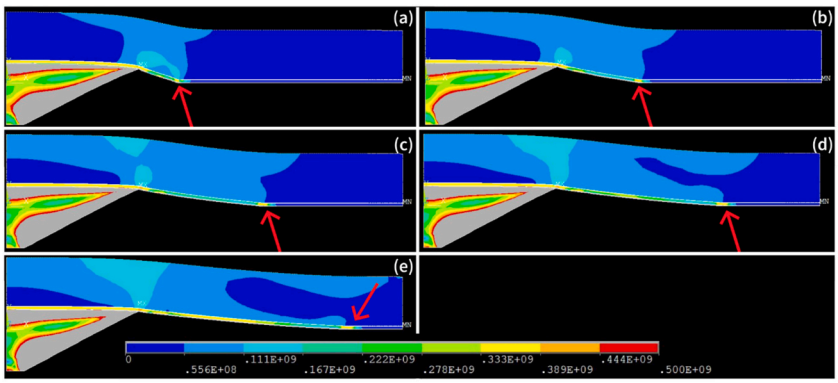

Fig. 10. Evolution of the von Mises stress (Pa) in the layers during the simulated crack growth ($N = 274$). The arrow indicates the current position of the crack tip for steps 100–500 of the performed simulation (out of a total of 550 steps) in images (a)–(e) respectively. The maximum stress displayed has been set to 0.5 GPa to better show the overall behavior of the system.

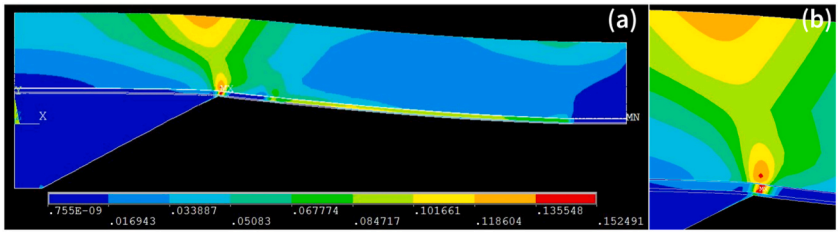

Fig. 11. von Mises strain (%) in the sample at the final step of crack extension ($N = 274$). An overview over the complete sample is given in (a) and a zoom in on the critical area where cracks initially kink into the interfaces in (b).

Table 3
Error in wedge displacement for experiments using the cube-corner tip at various distances caused due to imperfect crack closure ($\Delta u_{0,ct}$) and due to plasticity around the Si wedge ($\Delta u_{0,wp}$).

Distance (μm)	u_0 (μm)	$\Delta u_{0,ct}$ (μm)	$\Delta u_{0,wp}$ (μm)
8	0.89 ± 0.35	0.16 ± 0.16	0.051 ± 0.146
10	1.76 ± 0.47	0.40 ± 0.19	0.25 ± 0.26
12	2.86 ± 0.37	0.80 ± 0.29	0.69 ± 0.13

release rate against the number of elements along the crack path are shown in Fig. 12 with adjusted R^2 values between 0.995 and 0.997. This supports the expected exponential trend that was proposed in eq. (5). The convergence of the material is further shown with the open symbols that were obtained using said relation and are in saturation. Considering the close match and for the sake of faster convergence of the FEA, ΔN was increased to 96 and only four different mesh sizes per input set were considered for all other simulations performed in this study.

To better account for outliers the median value for each simulation at a set value N was taken for fitting. As seen in Fig. 13 this results in a value for the critical energy release rate via extrapolation $G_{c0CC} = 9.61 \pm 0.31$ J/m^2 at an average mode mixity of $\psi_{CC} = 59.71 \pm 4.58°$. The decrease of the median critical energy release rate between the most refined simulations at 370 elements compared to the extrapolated value is 2.83 %.

3.3. Observations for Berkovich tip geometry

Analogous investigations were performed on the 116 cracks created using the Berkovich indenter, from which 23 % could be evaluated using the mesh refinement method. In contrast to measurements done using the cube-corner indenter the indents at distance 10 μm yielded best results, while crack propagation at distances set to 8 μm was often minimal, exhibiting the lowest success rate for the Berkovich geometry. More than half of these cracks reached values of $\lambda > 1.7$ or did not propagate at all. At a distance of 12 μm, cracks could be reliably provoked, however they tended to kink out of the Si/SiO_x interface early and a significant amount of energy

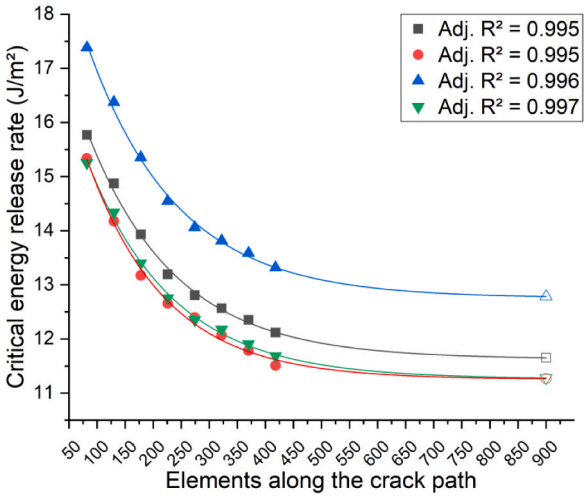

Fig. 12. Extrapolation of G_c values for various meshes to investigate the applicability of extrapolation to determine a mesh independent G_{c0}. The open symbols represent values obtained from extrapolation (using eq. (5)) that are in saturation but cannot be reached by using FEA.

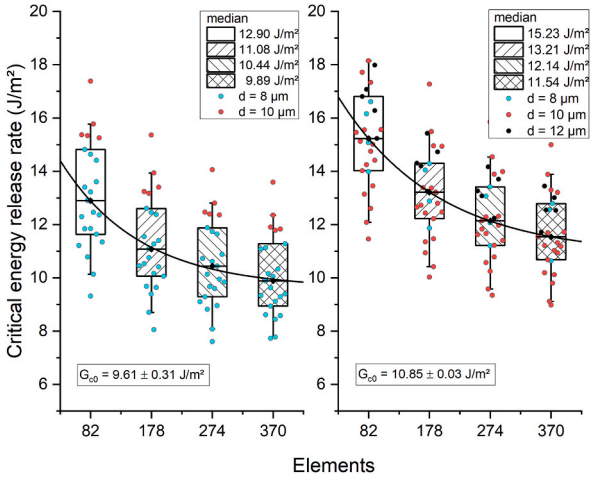

Fig. 13. Results for FEA simulations at various mesh sizes (a) for experiments performed using a cube-corner tip (b) for experiments performed using a Berkovich tip.

was invested into undesirable micro cracking of the Si substrate around the point of indentation. Consequently, the observed values of the critical energy release rate tend to be significantly higher than for the experiments performed at different settings. A detailed list of results is shown in the supplementary material.

The force needed to initiate cracking and the maximum velocity obtained, showed a linear increase with the distance to the interface (compare Fig. 9), albeit at significantly lower rate and initial values compared to the values obtained for the cube-corner tip. An additional error was found in the final crack opening caused by cracks kinking out of the intended interface, which is similar to what was observed with the cube-corner indenter. Table 4 shows this error depending on the selected distance to the interface. Analogous to the method used for the cube-corner indents, the values of u_0 were manually corrected before simulation. Using the obtained SEM images the angle of incidence of the crack into the deposited layers was measured to be $\omega = 32.07 \pm 3.5°$. Observations for indents performed with the Berkovich tip also showed a higher average load needed for delamination and significantly higher damage in the form of fracture of the Si wedge shown in Fig. 7(f). This, in turn, can cause debris to become wedged between the substrate and the delaminated layers, thus preventing proper crack closure after removal of the Berkovich tip as depicted in Fig. 7(e).

Results for FEA simulations at different mesh sizes are shown in Fig. 13 resulting in a value for the critical energy release rate via extrapolation $G_{c0Berk} = 10.86 \pm 0.03$ J/m^2 at an average phase angle $\psi_{Berk} = 60.1 \pm 8.02°$. The percentage decrease of the critical energy release rate between the simulation at 370 elements compared to the extrapolated value is 5.98 % for the Berkovich tip.

4. Discussion

4.1. Critical energy release rate and FEA simulations

The mesh size dependent values of G_c obtained by FE simulations in Fig. 12 show good agreement with the proposed exponential fit in eq. (5) allowing to obtain mesh independent values for the critical energy release rates reliably. The variations between the finest mesh and the extrapolated value are in good agreement with each other for both tip types, suggesting that the simulations are close to the saturation value. Obtained results for the FEA simulation presented in Figs. 10 and 11 show good agreement with the experimentally observed behavior depicted in Fig. 7. Especially the very high stresses in the silicon wedge (beyond 1 GPa in Fig. 10) show why both, the cracks initially propagate and why local fracture around the silicon wedge is occurring in some indentation experiments (as shown in Fig. 7(f)). Similarly, the distribution of the strain, shown in Fig. 11 explains the behavior at the very beginning of the crack advance, showing that the maximum strain is concentrated at just this point, in the aluminum layer and extends outwards into the polyimide. If sufficiently high strains are encountered for a specific experiment, striations in the polyimide or local deformation of the aluminum layer, as encountered in Fig. 7(d) can occur.

The results of the experiments with cube-corner tip and Berkovich tip are in relatively good agreement with a difference of only 1.25 J/m^2 for the extrapolated critical energy release rate. The values obtained at the same number of elements (N) are significantly higher for experiments employing the Berkovich tip and seem to be further away from reaching convergence than their cube-corner counterparts. The differences in the convergence behavior alone cannot explain the increase in the obtained values, rather it is also assumed that differences in the geometry of the indent and crack growth behavior influence the critical energy release rate, which will be described in more detail below.

4.2. Influence of tip geometry and distance

The first significant difference between experiments performed with different indenter tip geometries is the force required to

Table 4
Error in wedge displacement for experiments using the Berkovich tip at various distances caused due to imperfect crack closure ($\Delta u_{0,ct}$) and due to plasticity around the Si wedge ($\Delta u_{0,wp}$).

Distance (μm)	u_0 (μm)	$\Delta u_{0,ct}$ (μm)	$\Delta u_{0,wp}$ (μm)
8	0.575 ± 0.34	0.20 ± 0.06	0
10	1.38 ± 0.47	0.30 ± 0.16	0.085 ± 0.147
12	1.69 ± 0.70	0.37 ± 0.23	0.079 ± 0.145

initiate cracking. For the same distance to the interface the cube-corner geometry requires, on average, 52 %–61 % less force to initiate cracking, during CSN experiments, compared to the same experiments performed with the Berkovich tip as seen in the clear distinction between the two data sets for the tip geometries in Fig. 9. This can be attributed to the steeper opening angle of the cube-corner tip, facilitating easier crack initiation in the substrate [40]. Due to this, a shift of the optimal settings is observed, where successfully evaluated experiments (crossed datapoints in Fig. 9) for the cube-corner geometry cluster at smaller pop-in loads below 80 mN achieved mainly at smaller distances, while for the Berkovich tip, the optimal window for the pop-in loads shows a wider range between 120 and 220 mN.

Experiments performed with the cube-corner tip show the highest success rate at a set distance of 8 μm, limited success at set distances of 10 μm and no success at any higher distances. In contrast, the Berkovich tip shows successes at all tested distances, but primarily at 10 μm. Experiments performed at set distances of 12 μm show a highly overestimated critical energy release rate and a slightly lower success rate, including experiments with overestimated critical energy release rates by the FEA. On the contrary, cracks at distances of 8 μm often did not propagate sufficiently to serve as an input for the FEA routine. A detailed list of success rates sorted by set distances can be found in Table 5.

Influences of the indentation distance from the interface on the critical energy release rate was already described by Sánchez et al. [10] in their original paper describing the CSN method. They proposed that the dependence is due to the strain-affected zone surrounding the point of indentation on the deposited layers. To investigate this possible effect, a relation proposed by Jang and Pharr [37] was employed, which relates the plastic zone size of an indent to the geometry of the indentation mark and the material properties of the indented substrate as shown in eq. (6)

$$p = \frac{1}{1.48} \cdot a \cdot \left(\frac{E}{H}\right)^{\frac{1}{2}} \cdot \left(\frac{3\sqrt{3}}{16 \cdot \pi}\right)^{\frac{1}{3}} \cdot cot^3(\Theta) \tag{6}$$

where p describes the hemispherical plastic zone size, a the indentation mark size from center to corner, Θ the half angle of the nanoindentation tip, E and H the Young's modulus and hardness of the indented material respectively.

For a possible effect of plasticity in the deposited layers along the crack path the plastic zone size p must satisfy the following inequality which, based on geometric considerations (compare Fig. 3), corresponds to the distance from the point of indentation to the point where the delamination of the interface starts

$$p \geq \sqrt{b^2 + d^2} \tag{7}$$

here d is the set distance from the interface (8 μm, 10 μm or 12 μm) and b half the width of the fractured Si-wedge.

Due to the combination of the small indentation mark size, the set distances to the interface and the properties of the silicon substrate (hardness $H = 11\ GPa$ as measured by nanoindentation) the condition for eq. (7) is not satisfied for either tip geometry and therefore no effects on the deposited layers are expected to occur.

A Comparison of the current study to similar studies on other thin film layered systems provides a more likely explanation for the observed differences in the critical energy release rate. In the absence of the thick polyimide layer, optimal settings for delamination using the Berkovich-tip are in the range of loads below 120 mN and at significantly lower distances of 1–7 μm compared to the current study [10,24,41]. For the present system, tests at such distances did not yield any useable results, but rather an immediate kinking of the crack into the Al layer. This is shown by the high values of the ratio between the Si wedge width and the final crack length in such tests, especially at 8 μm distance for the Berkovich tip geometry. However, moving to higher distances for indentation experiments increases the risk of inducing unwanted micro cracking around the point of indentation (Fig. 7(f)).

The effect of this fracture on the resulting delamination is twofold. Firstly, in such cases the energy input by nanoindentation is not

Table 5
Success rates for both tip geometries depending on the distance to the interface.

Tip	Set Distance (μm)	#Cracks	Success rate (%)
Cube-corner	8	60	32
	10	58	7
	12	10	0
Berkovich	8	28	14
	10	60	30
	12	28	25

only consumed by crack propagation but also by the cohesive fracture of the Si. Secondly debris can be wedged in-between the two delaminated layers (Fig. 7(e)), which keeps the cracks from closing and thus increasing the value of u_0 obtained by SEM imaging. Both effects are difficult to consider in the FEA simulations and can lead to a systematic error in the results obtained for such indents. We assume that these two effects are the main reason for higher values of the energy release rate generated with the Berkovich tip at distances of 12 μm and to some extent at 10 μm.

In this regard the cube-corner geometry is more advantageous for the current material system, as cracks occur at lower loads and therefore do not provoke micro cracking around the point of indentation in the Si substrate. Still, it is important to also emphasize the disadvantages of using a cube-corner tip for CSN experiments, where unwanted effects do not occur in the Si-substrate but rather in the deposited layers around the separated Si segment. This effect which is shown in Fig. 7(d) in the form of damage in the polyimide layer and local deformation of the other layers are reflected in the FEA simulation and can lead to divergence of the simulation. Therefore, a more precise choice of the distance to the interface is necessary for such experiments, which is evident in the fact that success rates are low at distances of 10 μm and zero at distances of 12 μm when using cube-corner tips.

It was initially assumed that this local deformation is caused by the difference in the angles of incidence of the crack on the interface between the two tip geometries [42]. However, both tips show comparable behavior and impinge on the interface at approximately the same angle of $\omega = 35°$. This suggests that the local increase in u_0 around the wedge is produced after the final crack length has been reached and after the Al- and polyimide layer have sufficiently plastified at the crack tip. If the tip has not come to a halt at this point, the remaining energy is invested into local deformation around the wedge. Since the tip with Berkovich geometry does not reach peak velocities as high as the cube-corner tip, this phenomenon is less pronounced in these instances, which is in agreement with our results when comparing the errors reported in Table 3 for the cube-corner tip to those in Table 4 for the Berkovich tip.

A further point, especially when comparing CSN to other methods is the mode mixity. Previous investigations of CSN show mode mixity angles of $\psi = 50°$ [23,24,41], while significantly higher mode mixities of $\psi_{CC} = 59.33°$ and $\psi_{Berk} = 60.1°$ were observed in the current study. Whilst the values for the cube-corner and Berkovich tip closely align for the current system, there is an increase by approximately 10° compared to the literature reference. Using the relation $\tau_{xy}/\sigma_{yy} = \tan(\psi)$ the ratio of shear-to tensile stress can be calculated to be $\tau_{xy}/\sigma_{xx} = 1.73$ during the crack growth process compared to the expected $\tau_{xy}/\sigma_{xx} = 1.19$ obtained using values form the literature.

Hutchinson and Suo [20] proposed phenomenological models to describe the behavior of G_c with regard to the mode mixity by introducing a weight-factor λ ranging from 0 to 1 for the contribution of the shear component. Under the assumption of no crack propagation due to mode II cracking ($\lambda = 0$), Pape et al. [38] simplified the relation to

$$G_c(\psi) = G_c(0°)/\cos^2(\psi) \tag{8}$$

which allows for a rough estimation of the obtained values of the critical energy release rate to the minimum values obtained at pure mode I propagation. Eq. (8) suggests that critical energy release rate values obtained in this study, with mode mixity angles of approximately $\psi = 60°$, are 4 times higher than values obtained at pure mode I crack propagation. Meanwhile, values at $\psi = 50°$ only lead to a relative increase of 2.4 times. As Pape et al. state themselves, their assumptions are only valid for ideal solids and not for interfaces in real-life materials. Hence, the influence of the mode mixity on the results discussed here describes an upper limit. For a more detailed investigation, different experimental methods have to be compared, as was for example done by Walter et al. [43] for the investigation of polyimide copper adhesion.

4.3. Influence of the loading rate & indenter tip velocity

For both types of tips used for the experiments, no considerable influence of the loading rate on the experimental results could be determined. This can be attributed to the fact, that the delamination starts as soon as the Si wedge separates from the bulk, at which point the loading rate is overshadowed by the acceleration of the nanoindenter tip due to the stored energy in the nanoindenter column being converted into kinetic energy. As more energy is stored when cracking occurs at higher loads, the load required for crack initiation might be a good indicator of the maximum indenter velocity reached during the indentation experiment (still strongly dependent on the used indenter tip geometry). This is in agreement with the trend seen in Fig. 9, where the successfully evaluable indentation experiments are concentrated in a characteristic window for each of the two tip geometries, which is narrower for the cube-corner geometry (50–65 mN) than for the Berkovich geometry (121–220 mN). The only reasonable influence of the loading rate could be phase transformations of the monocrystalline Si substrate from diamond structure to a β-tin type, which however are limited to loading rates below 30 μN/s [44]. As the loading rates used in this study are significantly higher, no influence is expected, and no characteristic jumps in the load displacement curve that would appear due to a volume change during the phase transformation were observed.

Cut-off values for the indenter tip velocity were significantly surpassed in all experiments, which show that this value cannot be taken as a finely tunable value but rather as a limit. The cut-off value should be set with caution. Setting a too low value can lead to premature termination of the test before delamination sets in, while setting a too high one can lead to the load plateau not being recognized, with both effects leading to failure of the test. Nevertheless, using the indenter tip velocity and a cut-off value seems to be the most promising way to automate testing and data acquisition, where a batch of indentation experiments along the interface can be performed without input of the user and tedious setting of a maximum load or other parameters. This combined with the fact that sample preparation is fast and requires little input from the user makes CSN attractive, even though the success rate remains moderate.

5. Conclusion

To achieve successful adhesion measurements of the Si/SiO_x/Al/Si_xN_y/polyimide stack by cross sectional nanoindentation with subsequent finite element analysis the following important parameters have been found.

(i) The distance from the interface for cube-corner indentation should be smaller (8 μm) than that for Berkovich indentation (10 μm) to induce significant delamination without adverse effects.
(ii) For experiments with the Berkovich tips more damage in the Si substrate is observed compared to the ones with the cube-corner indenter. In the latter case the deformation and damage are confined to the delaminated layers.
(iii) The finite element analysis (FEA) results were found to be mesh dependent; an extrapolation approach is needed obtain meaningful values.
(iv) Only high-quality cube-corner indentation experiments can be evaluated by FEA due to effects described in (ii).

CRediT authorship contribution statement

Moritz Hartleb: Writing – original draft, Visualization, Software, Investigation, Formal analysis, Data curation. **Peter Imrich:** Writing – review & editing, Supervision, Resources, Project administration, Funding acquisition, Conceptualization. **Johannes Zechner:** Writing – review & editing, Supervision, Conceptualization. **Thomas Walter:** Supervision, Methodology. **Manuel Petersmann:** Validation, Software. **Golta Khatibi:** Writing – review & editing, Conceptualization.

Data availability

Selected data will be made available on request. Raw simulation data cannot be shared due to file size.

Declaration of competing interest

The authors declare that they have no known competing financial interests or personal relationships that could have appeared to influence the work reported in this paper.

Acknowledgements

This work was funded by the Austrian Research Promotion Agency (FFG, Project No. 905107). The authors acknowledge TU Wien Bibliothek for financial support through its Open Access Funding Programme.

Appendix A. Supplementary data

Supplementary data to this article can be found online at https://doi.org/10.1016/j.heliyon.2024.e40967.

References

[1] J. Chen, S.J. Bull, Approaches to investigate delamination and interfacial toughness in coated systems: an overview, J. Phys. D Appl. Phys. 44 (3) (Jan. 2011) 034001, https://doi.org/10.1088/0022-3727/44/3/034001.
[2] K. Mittal, Adhesion measurement of thin films, Electrocomponent Sci Technol 3 (Jun. 1976), https://doi.org/10.1155/APEC.3.21.
[3] Z. Chen, K. Zhou, X. Lu, Y. Lam, A review on the mechanical methods for evaluating coating adhesion, Acta Mech. 225 (Feb. 2014), https://doi.org/10.1007/s00707-013-0979-y.
[4] "'Standard test methods for pull-off strength of coatings using portable adhesion testers,'ASTM D4541-22,in Book of Standards,vol. 6.2,DOI:10.1520/D4541-22.".
[5] "'Standard test method for adhesion strength and mechanical failure modes of ceramic coatings by quantitative single point scratch testing,'ASTM C1624-22,in Book of Standards,vol. 15.1,DOI: 10.1520/C1624-22.".
[6] "'Standard test methods for rating adhesion by tape test,'ASTM d3359-23,in Book of Standards,vol. 06.01,DOI: 10.1520/D3359-23.".
[7] P.G. Charalambides, J. Lund, A.G. Evans, R.M. McMeeking, "A test specimen for determining the fracture resistance of bimaterial interfaces,", J. Appl. Mech. 56 (1) (Mar. 1989) 77–82, https://doi.org/10.1115/1.3176069.
[8] A. Kleinbichler, M.J. Pfeifenberger, J. Zechner, S. Wöhlert, M.J. Cordill, "Scratch induced thin film buckling for quantitative adhesion measurements,", Mater. Des. 155 (Oct. 2018) 203–211, https://doi.org/10.1016/j.matdes.2018.05.062.
[9] Z. Peng, C. Wang, L. Chen, S. Chen, Peeling behavior of a viscoelastic thin-film on a rigid substrate, Int. J. Solid Struct. 51 (25) (Dec. 2014) 4596–4603, https://doi.org/10.1016/j.ijsolstr.2014.10.011.
[10] J.M. Sánchez, et al., Cross-sectional nanoindentation: a new technique for thin film interfacial adhesion characterization, Acta Mater. 47 (17) (Nov. 1999) 4405–4413, https://doi.org/10.1016/S1359-6454(99)00254-2.
[11] A.G. Varias, Z. Suo, C.F. Shih, Ductile failure of a constrained metal foil, J. Mech. Phys. Solid. 39 (7) (Jan. 1991) 963–986, https://doi.org/10.1016/0022-5096(91)90014-F.
[12] M.J. Cordill, F.D. Fischer, F.G. Rammerstorfer, G. Dehm, Adhesion energies of Cr thin films on polyimide determined from buckling: experiment and model, Acta Mater. 58 (16) (Sep. 2010) 5520–5531, https://doi.org/10.1016/j.actamat.2010.06.032.
[13] D. Gutnik, A. Kleinbichler, P.J. Imrich, M.J. Cordill, A. Lassnig, Adhesion of WTi to polyimide measured by complementary methods, Surf. Coating. Technol. 475 (Dec. 2023) 130148, https://doi.org/10.1016/j.surfcoat.2023.130148.

[14] A.A. Taylor, M.J. Cordill, L. Bowles, J. Schalko, G. Dehm, An elevated temperature study of a Ti adhesion layer on polyimide, Thin Solid Films 531 (Mar. 2013) 354–361, https://doi.org/10.1016/j.tsf.2013.01.016.
[15] M.E. Grady, P.H. Geubelle, N.R. Sottos, Interfacial adhesion of photodefinable polyimide films on passivated silicon, Thin Solid Films 552 (Feb. 2014) 116–123, https://doi.org/10.1016/j.tsf.2013.11.085.
[16] S.-W. Zhu, C.-P. Shih, T.-C. Chiu, G.S. Shen, Delamination fracture characteristics for polyimide-related interfaces under fatigue loadings, in: 2010 5th International Microsystems Packaging Assembly and Circuits Technology Conference, Oct. 2010, pp. 1–4, https://doi.org/10.1109/IMPACT.2010.5699574.
[17] M. Hartleb, P. Imrich, J. Zechner, T. Walter, G. Khatibi, Cross-sectional Nanoindentation: applicability for testing Polyimide adhesion in semiconductor components, in: 2023 46th International Spring Seminar on Electronics Technology (ISSE), May 2023, pp. 1–5, https://doi.org/10.1109/ISSE57496.2023.10168521.
[18] G. Xu, M.-Y. He, D.R. Clarke, The effect of moisture on the fracture energy of TiN/SiO2 interfaces in multi-layer thin films, Acta Mater. 47 (15) (Nov. 1999) 4131–4141, https://doi.org/10.1016/S1359-6454(99)00272-4.
[19] M.D. Kriese, W.W. Gerberich, N.R. Moody, Quantitative adhesion measures of multilayer films: Part II. Indentation of W/Cu, W/W, Cr/W, J. Mater. Res. 14 (7) (Jul. 1999) 3019–3026, https://doi.org/10.1557/JMR.1999.0405.
[20] J.W. Hutchinson, Z. Suo, "Mixed mode cracking in layered materials,", in: J.W. Hutchinson, T.Y. Wu (Eds.), Advances in Applied Mechanics, vol. 29, Elsevier, 1991, pp. 63–191, https://doi.org/10.1016/S0065-2156(08)70164-9.
[21] S. McCann, et al., Determination of energy release rate through sequential crack extension, J. Electron. Packag. 139 (Aug. 2017) 041003, https://doi.org/10.1115/1.4037334.
[22] S. Huang, C. Zhou, Modeling and simulation of nanoindentation, JOM 69 (11) (Nov. 2017) 2256–2263, https://doi.org/10.1007/s11837-017-2541-1.
[23] M.R. Elizalde, et al., Interfacial fracture induced by cross-sectional nanoindentation in metal–ceramic thin film structures, Acta Mater. 51 (14) (Aug. 2003) 4295–4305, https://doi.org/10.1016/S1359-6454(03)00256-8.
[24] T. Walter, M. Zareghomsheh, G. Khatibi, H. Danninger, Adhesion properties of thin film multilayers: Comparison of nanoindentation and four-point-bending techniques, Mater. Sci. Forum 1016 (2021) 1561–1568, 10.4028/www.scientific.net/MSF.1016.1561.
[25] Delamination and fracture, in: L.B. Freund, S. Suresh (Eds.), Thin Film Materials: Stress, Defect Formation and Surface Evolution, Cambridge University Press, Cambridge, 2004, pp. 220–311, https://doi.org/10.1017/CBO9780511754715.005.
[26] J. Auersperg, R. Dudek, J. Oswald, B. Michel, Interaction integral and mode separation for BEoL-cracking and -delamination investigations under 3D-IC integration aspects, in: 2011 12th Intl. Conf. On Thermal, Mechanical & Multi-Physics Simulation and Experiments in Microelectronics and Microsystems, Apr. 2011, pp. 1/7–7/7, https://doi.org/10.1109/ESIME.2011.5765801.
[27] H. Guojun, A.A.O. Tay, "Application of modified virtual crack closure method on delamination analysis in a plastic IC package during lead-free solder reflow,", in: 2005 7th Electronic Packaging Technology Conference, Dec. 2005, p. 6, https://doi.org/10.1109/EPTC.2005.1614465.
[28] A. Agrawal, A.M. Karlsson, Obtaining mode mixity for a bimaterial interface crack using the virtual crack closure technique, Int. J. Fract. 141 (1–2) (Sep. 2006) 1–2, https://doi.org/10.1007/s10704-006-0069-4.
[29] E.F. Rybicki, M.F. Kanninen, A finite element calculation of stress intensity factors by a modified crack closure integral, Eng. Fract. Mech. 9 (4) (Jan. 1977) 4, https://doi.org/10.1016/0013-7944(77)90013-3.
[30] C. Fan, P.-Y. Ben Jar, J.J. Roger Cheng, Prediction of energy release rates for crack growth using FEM-based energy derivative technique, Eng. Fract. Mech. 74 (8) (May 2007) 8, https://doi.org/10.1016/j.engfracmech.2006.07.014.
[31] C. Durand, M. Klingler, D. Coutellier, H. Naceur, Study of fatigue failure in Al-chip-metallization during power cycling, Eng. Fract. Mech. 138 (Apr. 2015) 127–145, https://doi.org/10.1016/j.engfracmech.2015.02.020.
[32] H.-Y. Lin, S.P. Gurrum, Global and local characterization of passivated aluminum metallization film for extracting elastoplastic constitutive model, in: 2016 IEEE 66th Electronic Components and Technology Conference (ECTC), May 2016, pp. 766–773, https://doi.org/10.1109/ECTC.2016.289.
[33] Z. Xiujuan, C. Wanpeng, Finite element analysis for the effect of material properties on the punching of bimetal sheets, in: 2010 2nd International Conference on Education Technology and Computer, Jun. 2010, p. 71, https://doi.org/10.1109/ICETC.2010.5529595. V3-68-V3.
[34] Z. Chen, J. Chen, X. Hou, L. Chen, Mechanically robust and thermal-insulated polyimide aerogel films by polymerization-regulated strategy for flexible thermal protection, Chem. Eng. J. 496 (Sep. 2024) 154251, https://doi.org/10.1016/j.cej.2024.154251.
[35] H. He, J. Yin, L. Song, Q. Deng, High-temperature mechanical responses of the polyimide at a high strain rate, J. Phys.: Conf. Ser. 2535 (1) (Jun. 2023) 012016, https://doi.org/10.1088/1742-6596/2535/1/012016.
[36] D.-S. Liu, S.-S. Yeh, C.-T. Kao, H.-C. Shen, G.-S. Shen, H.-H. Liu, Optimization of bonding force, sinking value, and potting gap size in COF inner lead bonding process, IEEE Trans. Adv. Packag. 32 (3) (Aug. 2009) 593–601, https://doi.org/10.1109/TADVP.2009.2025671.
[37] J. Jang, G.M. Pharr, Influence of indenter angle on cracking in Si and Ge during nanoindentation, Acta Mater. 56 (16) (Sep. 2008) 4458–4469, https://doi.org/10.1016/j.actamat.2008.05.005.
[38] H. Pape, I. Maus, H.S. Nabi, L.J. Ernst, B. Wunderle, Establishing mode mix dependency of fracture toughness in microelectronic components with reduced experimental effort, in: 2012 IEEE 62nd Electronic Components and Technology Conference, May 2012, pp. 1213–1222, https://doi.org/10.1109/ECTC.2012.6248990.
[39] A.A. Volinsky, N.R. Moody, W.W. Gerberich, Interfacial toughness measurements for thin films on substrates, Acta Mater. 50 (3) (Feb. 2002) 441–466, https://doi.org/10.1016/S1359-6454(01)00354-8.
[40] T. Chudoba, P. Schwaller, R. Rabe, J.-M. Breguet, J. Michler, Comparison of nanoindentation results obtained with Berkovich and cube-corner indenters, Phil. Mag. 86 (33–35) (Nov. 2006) 5265–5283, https://doi.org/10.1080/14786430600746424.
[41] T. Walter, et al., Interfacial adhesion strength of III-N heterostructures, Mater. Des. 213 (Jan. 2022) 110319, https://doi.org/10.1016/j.matdes.2021.110319.
[42] M.-Y. He, J.W. Hutchinson, Crack deflection at an interface between dissimilar elastic materials, Int. J. Solid Struct. 25 (9) (1989) 1053–1067, https://doi.org/10.1016/0020-7683(89)90021-8.
[43] T. Walter, M. Lederer, G. Khatibi, Delamination of polyimide/Cu films under mixed mode loading, Microelectron. Reliab. 64 (Sep. 2016) 281–286, https://doi.org/10.1016/j.microrel.2016.07.100.
[44] L. Chang, L. Zhang, Mechanical behaviour characterisation of silicon and effect of loading rate on pop-in: a nanoindentation study under ultra-low loads, Materials Science and Engineering: A 506 (1) (Apr. 2009) 125–129, https://doi.org/10.1016/j.msea.2008.11.021.